


EXPRESS LETTER

Open Access



Influence of composition-dependent thermal conductivity on the long-term evolution of primordial reservoirs in Earth's lower mantle

Yang Li^{1*} , Frédéric Deschamps^{2*}, Zhidong Shi¹, Joshua M. Guerrero², Wen-Pin Hsieh², Liang Zhao¹ and Paul J. Tackley³

Abstract

The influence of composition-dependent thermal conductivity and heterogeneous internal heating of primordial dense material on the long-term evolution of primordial reservoirs in the lower mantle of the Earth is investigated utilizing thermochemical mantle convection simulations in a 2-D spherical annulus geometry. Our results show that a reduction in the thermal conductivity of primordial dense material due to iron enrichment does not substantially alter mantle dynamics nor the long-term stability of the reservoirs of this dense material. If the primordial dense material is also enriched in heat-producing elements, the average altitude of these reservoirs slightly increases as the thermal conductivity is reduced, therefore, covering smaller core–mantle boundary areas. Our study indicates that the composition-dependent thermal conductivity of primordial material plays a second order role in the long-term evolution of Earth's mantle.

Keywords: Mantle dynamics, Thermal conductivity, Lower mantle, Primordial reservoirs, Thermo-chemical mantle convection

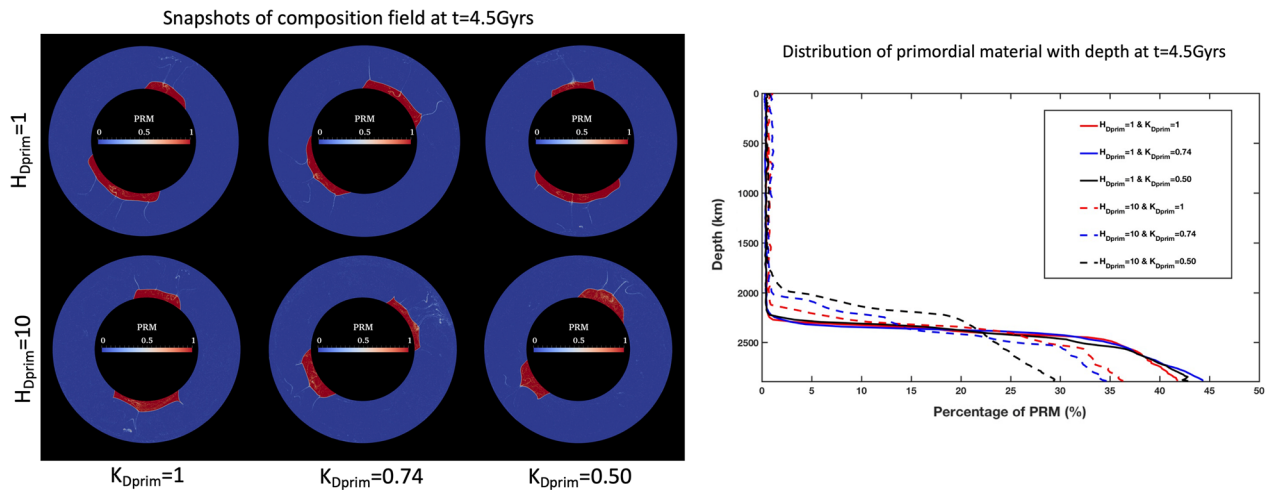
*Correspondence: yli@mail.iggcas.ac.cn; frederic@earth.sinica.edu.tw

¹ State Key Laboratory of Lithospheric Evolution, Institute of Geology and Geophysics, Institutions of Earth Science, Chinese Academy of Sciences, Beijing, China

² Institute of Earth Sciences, Academia Sinica, Taipei, Taiwan

Full list of author information is available at the end of the article

Graphical Abstract



Introduction

Seismological observations revealed the presence of two continental sized regions in the lowermost mantle, in which shear-wave velocity decreases by a few percent compared to the average velocity at these depths (e.g., He and Wen 2012; Ni et al. 2002; Ritsema et al. 2011). Interestingly, compressional-wave velocity in these regions is also reduced compared to horizontal average, a bit less (typically $\sim 1\%$) than shear-wave velocity (Houser et al. 2008; Ward et al. 2020). These so-called large low velocity provinces (LLVPs) are located beneath Africa and the Pacific, and they cover around 30% of core-mantle boundary (CMB) (see review by Garnero et al. (2016)). Tomographic models combining forward and inverse waveform modeling suggested that LLVPs may be less uniform than previously expected (French and Romanowicz 2014), forming bundles of thermochemical structures rather than thick and stable piles (Davaille and Romanowicz 2020). Whatever the exact structure of LLVPs, uniform piles or bundles, their nature, purely thermal or thermo-chemical, is still debated. While a purely thermal nature cannot be entirely ruled out on the basis of travel time seismic data only (Davies et al. 2012; Koelemeijer et al. 2017), additional data, including normal mode seismology (Ishii and Tromp 1999; Trampert et al. 2004), density anomalies estimated from solid Earth tide measurements (Lau et al. 2017), and joint inversion of shear wave velocity and attenuation (Deschamps et al. 2019; Konishi et al. 2020), suggest that they are more likely simultaneously hotter and chemically distinct (denser) than the ambient mantle. By contrast, Stoneley

mode data (Koelemeijer et al. 2017) points to light LLVPs, supporting a purely thermal origin for these structures. Assuming that LLVPs are chemically distinct and denser than surrounding mantle, interpretations of probabilistic tomography (Mosca et al. 2012; Trampert et al. 2004) indicate that LLVPs would fit the seismic observations well if they are enriched in iron by a few ($\sim 2\text{--}3\%$) percent. This iron enrichment may serve as a possible nature for LLVPs, since it can explain both the drop in shear velocity and the excess density observed by normal modes and tidal data. This density excess may, in turn, allow the persistence of LLVPs in mantle convection.

The thermal state of the lower mantle and its mineralogical composition may impact the physical properties of mantle rocks, altering mantle dynamics. For instance, viscosity, which depends on temperature, pressure and composition, strongly affects the flow. Thermal conductivity is another key physical property, as it affects heat transport across the mantle, and it is known to depend on temperature and pressure (Klemens et al. 1962). Numerical simulations of mantle convection usually assume a thermal conductivity that is either constant or pressure-dependent (Hansen et al. 1993; Li and McNamara 2018; Nakagawa et al. 2010; Zhong 2006). Some studies also employed a more detailed thermal conductivity varying with temperature and pressure (Schmeling et al. 2003; Tosi et al. 2013), and take into account multiple phase transitions that have been constrained by experimental studies of lower mantle minerals (Tosi et al. 2010). The conductivity of lower mantle further depends on its exact composition. Recent high pressure mineral physics

experiments indicated that the thermal conductivities of lower mantle minerals decrease with increasing iron content in bridgmanite (Hsieh et al. 2017) and ferropericlase (Hsieh et al. 2018; Ohta et al. 2017). Therefore, if LLVPs are enriched in iron by several percent compared to the ambient lower mantle, their thermal conductivity may be smaller than that of the ambient mantle (Hsieh et al. 2017). A recent analytical study combining experimental data and probabilistic tomography (Deschamps and Hsieh 2019) suggests that, compared to the surrounding mantle, the thermal conductivity may be reduced by up to 26% in LLVPs. However, the potential dynamic effects induced by lateral variations in thermal conductivity caused by such composition changes have not been addressed so far.

The origin of LLVPs is also not well understood. Although recycled mid-ocean ridge basalt (MORB) has been proposed to be one explanation (Christensen and Hofmann 1994; Brandenburg and Van Keken 2007), other studies pointed out that subducted MORBs in the lower mantle should result in high velocity rather than low velocity (Deschamps et al. 2012; Wang et al. 2020). As a result, LLVPs entirely composed of MORBs should be extremely hot (with excess temperature with respect to average mantle larger than 1000 K) to be able to create negative shear velocity anomalies of 2 to 3%, as observed by seismic tomography. Even so, Jones et al. (2020) shows that LLVP-like features with reasonable velocity contrasts can be produced from subducted MORB. Another possible origin of LLVPs is that they are reservoirs of primordial dense material that have formed at an early evolutionary stage of the Earth, and persisted since then (e.g., Dziewonski et al. 2010; Labrosse et al. 2007; Lee et al. 2010). Besides its heterogeneous composition, the mantle degree of heterogeneity in heat-producing elements (HPEs) remains largely uncertain. Estimates based on low heat-producing bulk silicate earth (BSE) do not require reservoirs enriched in heat-producing elements to explain the heat budget of mantle models (e.g., O'Neill and Palme 2008), while other studies (e.g., Hofmann 1997; Kellogg et al. 1999; White 2015) support the presence of reservoirs of undegassed (primordial) material enriched in heat-producing elements.

In this study, we perform numerical experiments in 2-D spherical annulus geometry to investigate the combined influence of a composition-dependent thermal conductivity and heterogeneous internal heating rate on the long-term evolution of primordial reservoirs in the Earth's lowermost mantle.

Method

In this study, we perform numerical experiments of thermo-chemical convection in an anelastic compressible fluid with infinite Prandtl number using the finite volume/difference code StagYY, which was thoroughly described in Tackley (2008). Our model setup is similar to that used in Li et al. (2014, 2015, 2019), which we briefly summarize below.

All experiments are run in 2-D spherical annulus geometry, which corresponds to the equatorial slice of a sphere (Hernlund and Tackley 2008). Spherical annulus differs from cylindrical geometry (which corresponds to a slice of a cylinder) in that its virtual thickness is not constant but increases with distance from the center. A free-slip boundary condition is employed at both the top and bottom boundaries. The number of radial and lateral grid points are 128 and 1024, respectively, with radial grid refinement at the top and the bottom of the domain, and at the boundary between the upper and lower mantle (660 km depth). The anelastic approximation involves the definition of a reference state, including radial profiles for temperature, density, thermal expansion, and thermal conductivity, which are here calculated using thermodynamic relationships for the Earth's mantle (Tackley 1998). Additional file 1: Fig. S1 plots this reference state. Note that thermal expansion decreases by a factor of 4 from surface to bottom.

The reference Rayleigh number is fixed at 10^8 in all experiments, and defined as

$$Ra_s = \frac{\alpha_s g \rho_s \Delta T_s D^3}{\eta_0 \kappa_s} \quad (1)$$

where α_s is the surface thermal expansivity, g the acceleration of gravity, ρ_s the surface density, ΔT_s super-adiabatic temperature difference, D the thickness of the mantle, η_0 the reference viscosity (taken at $T=1600$ K and depth $z=0$ km), and κ_s the surface thermal diffusivity. The viscosity depends on temperature, depth, composition, and yield stress. In addition, we imposed a viscosity jump of 30 between the upper and lower mantles. The viscosity is, therefore, fully given by

$$\eta = \frac{1}{\frac{1}{\eta_b(z,T)} + \frac{1}{\eta_Y}} \quad (2)$$

with

$$\eta_b(z, T) = \eta_0 [1 + 29H(z - 660)] \exp \left[E_a \frac{\Delta T_s}{T + T_{\text{off}}} + V_a \frac{z}{D} \right] \quad (3)$$

and

$$\eta_Y = \frac{\sigma_0 + \sigma_i P}{2\dot{\epsilon}} \quad (4)$$

where H is the Heaviside step function, V_a and E_a are the non-dimensional activation volume and activation energy, controlling viscosity variations with depth and temperature, respectively, and T_{off} is the offset temperature, which reduces the viscosity jump through the top thermal boundary layer. In all calculations, the value of T_{off} is set to $0.88 \Delta T_s$. The yield stress helps to emulate plate-like behavior at the top of the domain. Here, we defined the yield stress by imposing its surface value σ_0 , and its pressure gradient σ_i . The yield viscosity η_Y , is defined as the ratio between the yield stress and the second invariant of the strain rate tensor $\dot{\epsilon}$. To avoid numerical difficulties, the viscosity is truncated to a minimum of 10^{-3} and a maximum of 10^5 times the reference viscosity, η_0 .

The phase change from bridgmanite to post-perovskite (pPv) is included. All other conditions being the same, the viscosity of post-perovskite is identical to that of bridgmanite, i.e., the viscosity contrast between bridgmanite and post-perovskite is equal to 1. The pPv phase transition is modelled with a reference point defined at a temperature of 2700 K and a depth of 2700 km, and lateral deviations in the transition depth calculated following the phase function approach of Christensen and Yuen (1985). The Clapeyron slope and the density contrast are set to $\Gamma_{\text{pPv}} = 13$ MPa/K (Tateno et al. 2009) and $\Delta\rho_{\text{pPv}} = 62$ kg/m³ (Murakami et al. 2004), respectively. The stability field of pPv further depends on the temperature at the core-mantle boundary (CMB), T_{CMB} , which we fixed here to 3750 K. The phase change at 660 km is also taken into account with a Clapeyron slope $\Gamma_{660} = -2.5$ MPa/K, and a density contrast $\Delta\rho_{660} = 400$ kg/m³.

The composition field is tracked with the tracer ratio method by (Tackley and King 2003). Two types of tracers are used to calculate the compositional field, whose value varies between 0 for ambient mantle material and 1 for primordial material. Here, we used a total of 4 million tracers, corresponding to about 30 tracers per cell. The primordial material is initially distributed in a basal layer with a thickness of 0.07 (200 km in dimensional unit, Additional file 1: Fig. S2). The primordial material is set to be denser than the ambient mantle material, and the density contrast between primordial and ambient mantle materials is controlled by buoyancy ratio (B), which is defined as

$$B = \frac{\Delta\rho_c}{\alpha_s \rho_s \Delta T_s} \quad (5)$$

where $\Delta\rho_c$ is the density difference between the two types of mantle materials, respectively. In this study,

the buoyancy ratio is fixed to 0.30, corresponding to a dimensional chemical density contrast of 120 kg/m³. The evolution of the average altitude of primordial material, defined as

$$\langle h_C \rangle = \frac{1}{V} \int_V C(r - r_{\text{CMB}}, \theta)(r - r_{\text{CMB}}) dV \quad (6)$$

provides a good estimate of mixing efficiency. Small values of $\langle h_C \rangle$, around 0.04 in our case, correspond to stable layering, while large values, around 0.6, indicate efficient mixing.

The initial temperature profile is adiabatic with a potential temperature of 2000 K, and small random perturbations are added to initiate the convection (Additional file 1: Fig. S2). Fractionation of HPEs into primordial dense material is emulated by modifying its internal heating rate, relative to the internal heating rate of the ambient mantle, with an enrichment factor $H_{D\text{prim}}$. This leads to a distribution of internal heating rate, Rh , that varies with the amount of dense material according to the linear relationship:

$$Rh(C) = Rh_{\text{ref}} \times [1 + C(H_{D\text{prim}} - 1)] \quad (7)$$

where C is the concentration of dense tracers (compositional field varying, again between 0 and 1). In all calculations, the reference internal non-dimensional heating rate, Rh_{ref} is set to 14.8, corresponding to 4.0×10^{-12} W kg⁻¹. The total internal heating rate is equivalent to that calculated with Eq. (7) in which C is replaced by the volume fraction of dense material. Note that compressibility induces additional sources and sinks of heat that are controlled by the dissipation number.

A novelty, compared to previous models, is that the thermal conductivity is assumed to vary with the compositional field, the primordial materials differing by a factor $K_{D\text{prim}}$. This leads to the thermal conductivity varying according to the linear relationship:

$$k(C) = k_{\text{ref}}(z) \times [1 + C(K_{D\text{prim}} - 1)] \quad (8)$$

Following Eq. (8), values of $K_{D\text{prim}}$ lower than 1 decrease thermal conductivity compared to its horizontal average. Here, we tested two values of $K_{D\text{prim}}$, 0.74 and 0.5, leading to a reduction of conductivity by 26% and 50%, respectively. A reduction in conductivity of 26% accounts for the fact that primordial material may be enriched in iron by $\sim 3.0\%$ (Hsieh et al. 2017; Deschamps and Hsieh 2019), as expected in LLVPs (Trampert et al. 2004; Mosca et al. 2012). A reduction of 50% corresponds to a much stronger enrichment in iron (Hsieh et al. 2018), which might be the case for ultra-low velocity zones (ULVZs) if, for instance, these structures are the remnants of a basal magma ocean (Labrosse et al. 2007). The reference

thermal conductivity, $k_{ref}(z)$, is the same as that used in Li et al. (2015), and is plotted in Additional file 1: Figure S1. It increases linearly from top to bottom by about a factor of 2.5 with jumps at phase boundaries at 410 km, 660 km, and bridgmanite to post-perovskite. All other physical parameters used in this study are listed in Additional file 1: Table S1.

With this setup, simulations start with a long transient phase (around 0.6 Gyr), during which the bottom layer of dense material heats up, and are run up to a dimensional time of 4.5 Gyr. Our simulations are not meant to model the detailed evolution of the Earth's mantle, which would require the prescription of accurate initial conditions that are not yet known, and including a decaying rate of radioactive heating and dynamically evolving core–mantle boundary temperature in our models.

Results

We perform two series of numerical experiments, one with homogeneous internal heating (i.e., assuming that the primordial dense material contains the same amount of HPEs per unit mass as the ambient mantle), and the other one with heterogeneous internal heating (i.e., assuming that the primordial dense material contains 10 times more HPEs than the ambient mantle material per unit mass). In both series, we run three cases with different composition-dependent thermal conductivity ratios in primordial dense material: (1) a reference case with $K_{Dprim} = 1$, i.e., thermal conductivity of primordial dense material identical to that of the surrounding mantle; (2) a case with $K_{Dprim} = 0.74$, consistent with the conductivity reduction expected for LLVPs hotter than the surrounding mantle and enriched in iron by 3.0%; and (3) a case with $K_{Dprim} = 0.50$, corresponding to material strongly enriched in iron, as might be the case for ULVZs. It should be pointed out that, following the assumption that the reduction in conductivity is related to an enrichment in iron, prescribing a lower conductivity should imply that we also prescribe a slightly higher buoyancy ratio. However, because the buoyancy ratio is the dominant parameter in thermo-chemical convection, the effects induced by changing its value in accordance with the thermal conductivity would mask the individual effects due to thermal conductivity, if any.

Figure 1 shows results for the series with homogeneous internal heating. In each case, the thermochemical structures obtained at the end of an evolution of 4.5 Gyrs (Fig. 1a) are similar to the best observable fitting models obtained by Li et al. (2014) and Li et al. (2019), from which we borrow the parameters setup, and which mainly consist of two large reservoirs (or piles) of primordial material. For the three values of K_{Dprim} we tested, these thermochemical piles remain stable. Their structures are

broadly similar to each other, but differ slightly in their details. Figure 1b, plotting the evolution of averaged mantle temperature as a function of time, shows that the average temperatures for these three simulations are also very similar to each other. After the onset of convection, the cooling rates are about 75 K/Gyr for all cases. Note that the onset of the convection, which occurs around 0.6 Gyr, is slightly delayed, by up to ~ 0.06 Gyr, as the thermal conductivity of primordial dense material decreases. During this early stage, the system is fully stratified (CMB is fully covered by a layer of dense material) and heat is transferred by conduction. The short delay in the onset of convection may then be a consequence of the lower thermal conductivity, which reduces the CMB heat flux, as illustrated in Figs. 1 and 2, and lowers heat conduction within the basal layer. Decrease in CMB heat flux and heat conduction, in turn, are delaying the heating of the initial basal layer of dense material. Finally, as for the averaged mantle temperature, the evolutions of surface and CMB heat flows as functions of time (Fig. 1c) are broadly similar to each other. This is somewhat counter-intuitive, as one would expect heat flux to decrease with decreasing piles' thermal conductivity. However, because piles are also very hot, the heat flux in this region is already low, such that a reduced conductivity does not significantly alter the global heat flux. A close examination of the evolution of heat fluxes further indicates that the time-averaged heat flux slightly decreases with decreasing thermal conductivity of primordial material. These results suggest that a composition-dependent thermal conductivity does not substantially alter the pattern of convection and the stability of primordial reservoirs, or the thermal evolution of the system.

We then performed a second series of experiments in which the internal heating rate of primordial material is increased by a factor of 10 compared to the ambient mantle material. Figure 2a shows the thermochemical structures at the end ($t = 4.5$ Gyrs) of each simulation. Overall, the primordial reservoirs for cases with regular and reduced thermal conductivities are again similar to each other, and the pattern still consists of two stable thermochemical piles. However, the detailed structures slightly differ. As their thermal conductivity is reduced, the edges of the thermochemical piles become much steeper, and their altitude larger. Figure 2b, showing the evolution of averaged mantle temperature as a function of time, indicates that the secular cooling of the mantle is, again, similar in all cases. However, compared to the simulations with homogeneous internal heating, the delay of the onset of the convection is reduced. Figure 2c shows the time evolution of surface and CMB heat flows. The CMB heat flows are close to each other and are comparable, but slightly smaller than in the simulations with

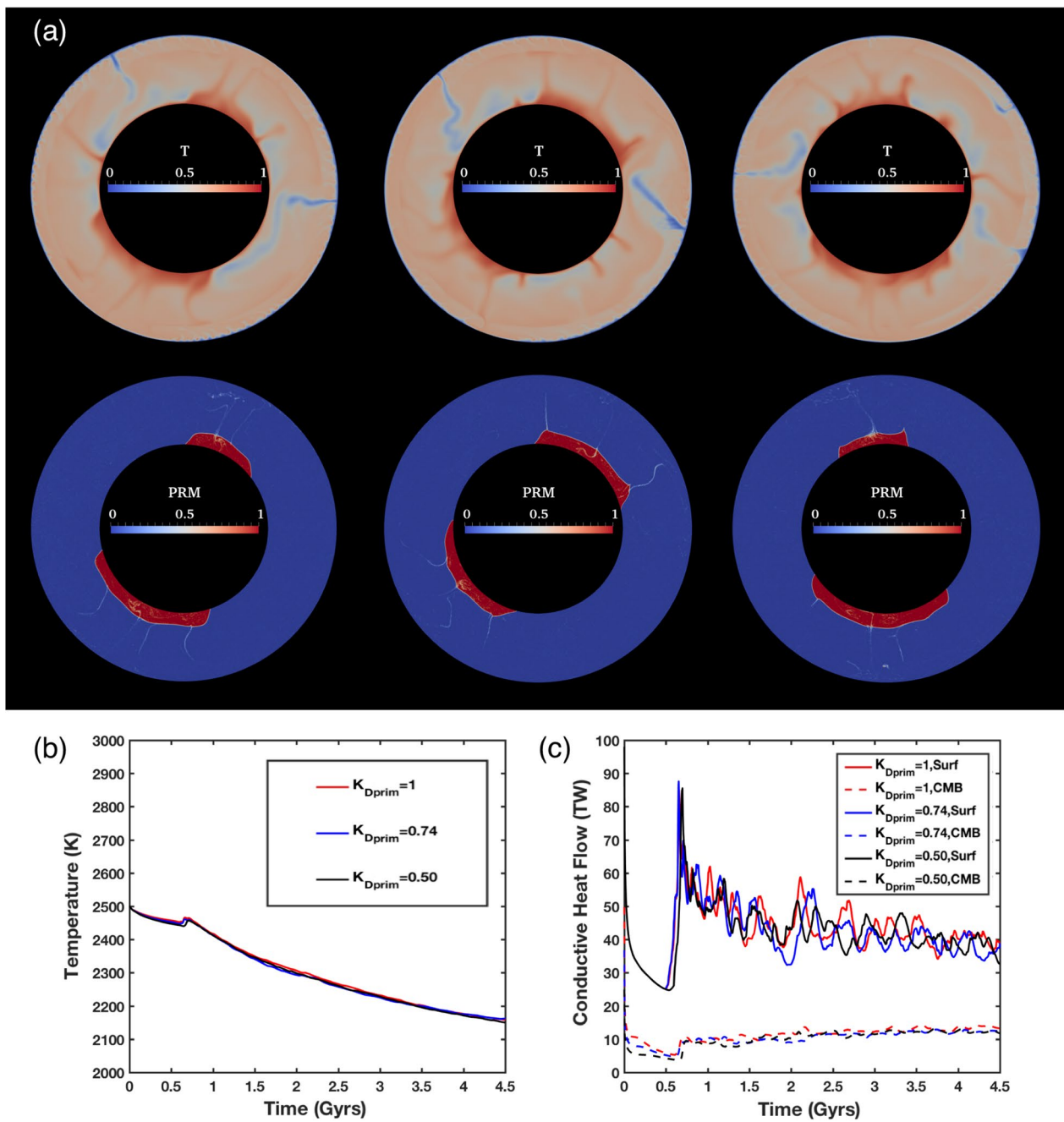


Fig. 1 $H_{Dprim} = 1$, **a** snapshots of non-dimensional superadiabatic temperature (top) and composition (bottom) fields at $t = 4.5$ Gyrs: from left to right K_{Dprim} varies from 1, 0.74, 0.5. **b** Averaged mantle temperatures as a function of time. **c** Surface and bottom heat flows as a function of time

homogeneous heating, around 10 TW. Furthermore, the surface heat flows are slightly larger, around 40 TW (compared to 38–39 TW for $H_{Dprim} = 1$), due to stronger plumes that form at the top of the hotter primordial reservoirs. As a result, the averaged mantle temperatures drop slightly faster, by about 5 K/Gyr, than those in the simulations with $H_{Dprim} = 1$.

Figure 3a shows horizontally averaged profiles of the fraction of primordial material, $\langle C \rangle$, for all six simulations at 4.5 Gyrs. The sharp transition between high average fraction (typically 20–30%, in the case of our simulations) and fraction around 1% or less denotes the top of the reservoirs of primordial material. For the experiments with homogeneous internal heating ($H_{Dprim} = 1$),

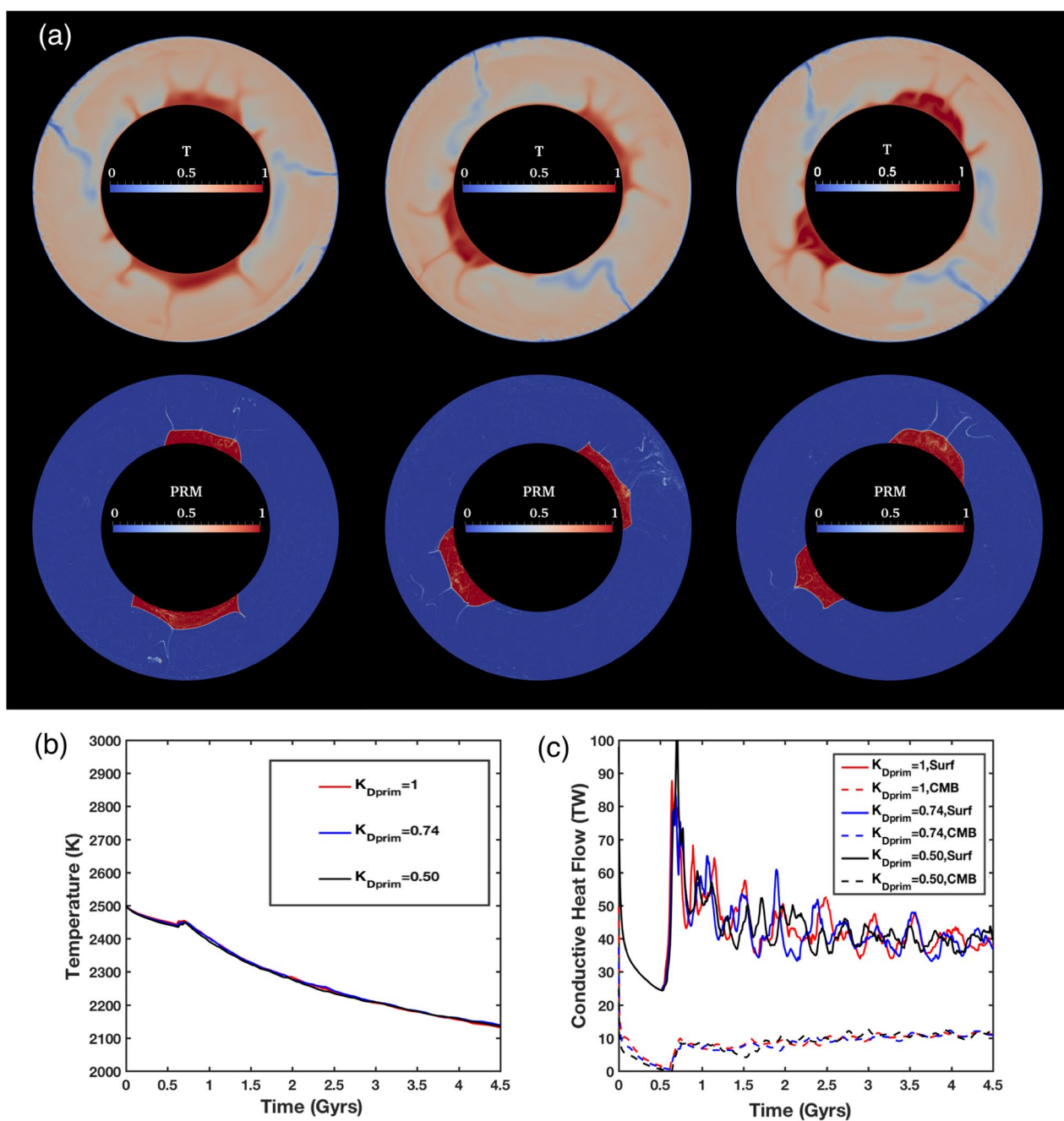


Fig. 2 $H_{Dprim} = 10$, **a** snapshots of non-dimensional superadiabatic temperature (top) and composition (bottom) fields at $t = 4.5$ Gyrs: from left to right K_{Dprim} varies from 1, 0.74, 0.5. **b** Averaged mantle temperatures as a function of time. **c** Surface and bottom heat flows as a function of time

the heights of these reservoirs are close to each other independently of the thermal conductivity of primordial material. The shape of these profiles is typical of piles with flat tops, in good agreement with the structures observed in Fig. 1a, and indicate that these piles extend up to about 600 km above the CMB. For experiments with heterogeneous internal heating ($H_{Dprim} = 10$), the

transition between high and low $\langle C \rangle$ is more progressive, indicating that piles have more topography, as can be seen in Fig. 2a. In addition, primordial reservoirs extend higher as the thermal conductivity of primordial material decreases. The heights of these reservoirs increase by 50 to 200 km compared to those with $H_{Dprim} = 1$, and the fraction of the CMB area covered by primordial

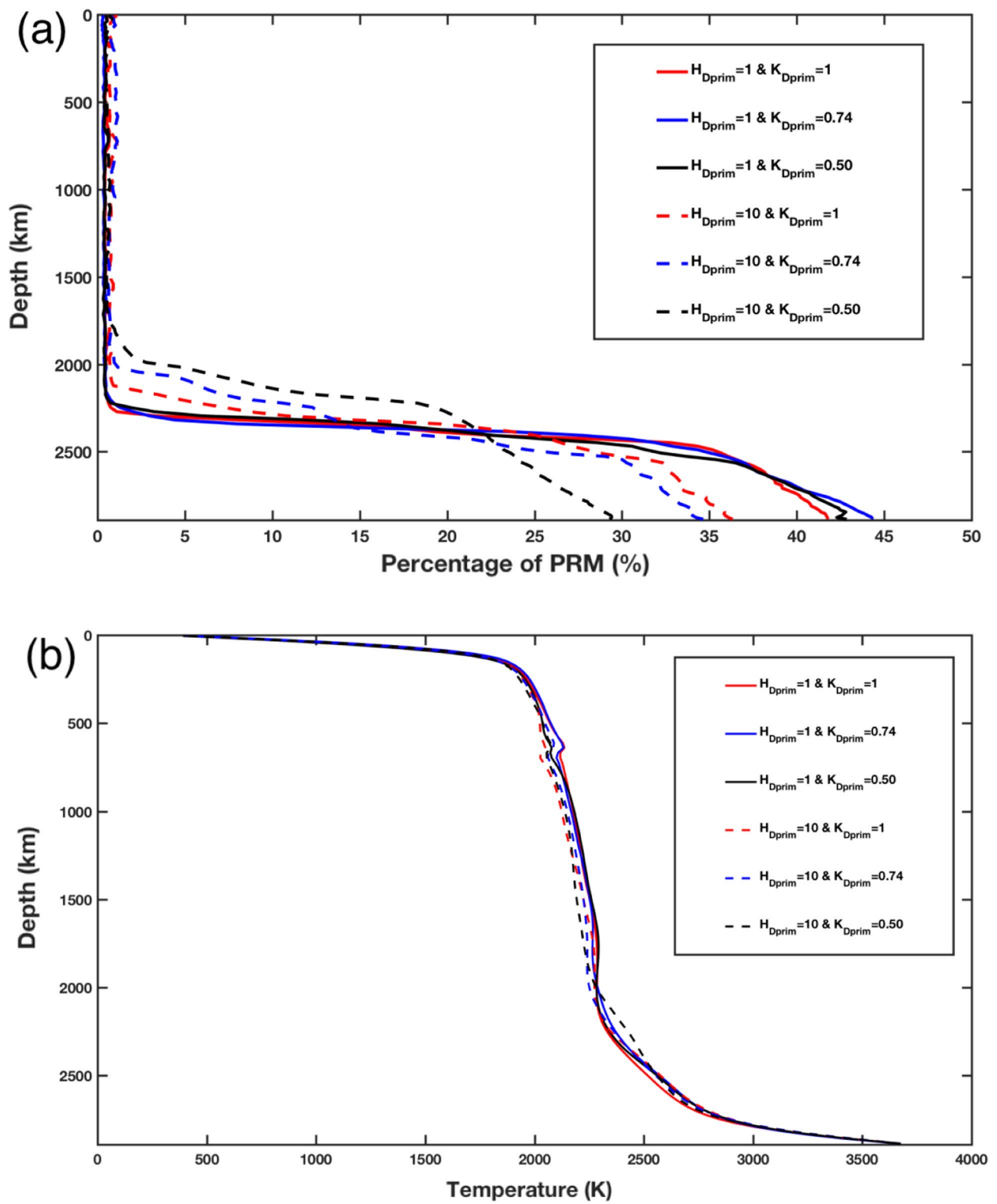


Fig. 3 **a** 1-D profiles of distributions of primordial material with depth at $t = 4.5$ Gyrs; **b** 1-D profile of averaged mantle temperature with depth at $t = 4.5$ Gyrs

reservoirs decreases by up to 20% (compared to 5% for the homogeneous heating cases) for decreasing K_{Dprim} . Increasing the internal heating rate of primordial material, therefore, enhances the role played by heterogeneous thermal conductivity, with lower conductivity leading to warmer, less stable piles. Figure 3b shows the averaged mantle temperature with depth, and indicates that the temperature differences are rather small among all these cases. Figure S3 shows radial profiles of horizontally averaged viscosity are also similar to each other.

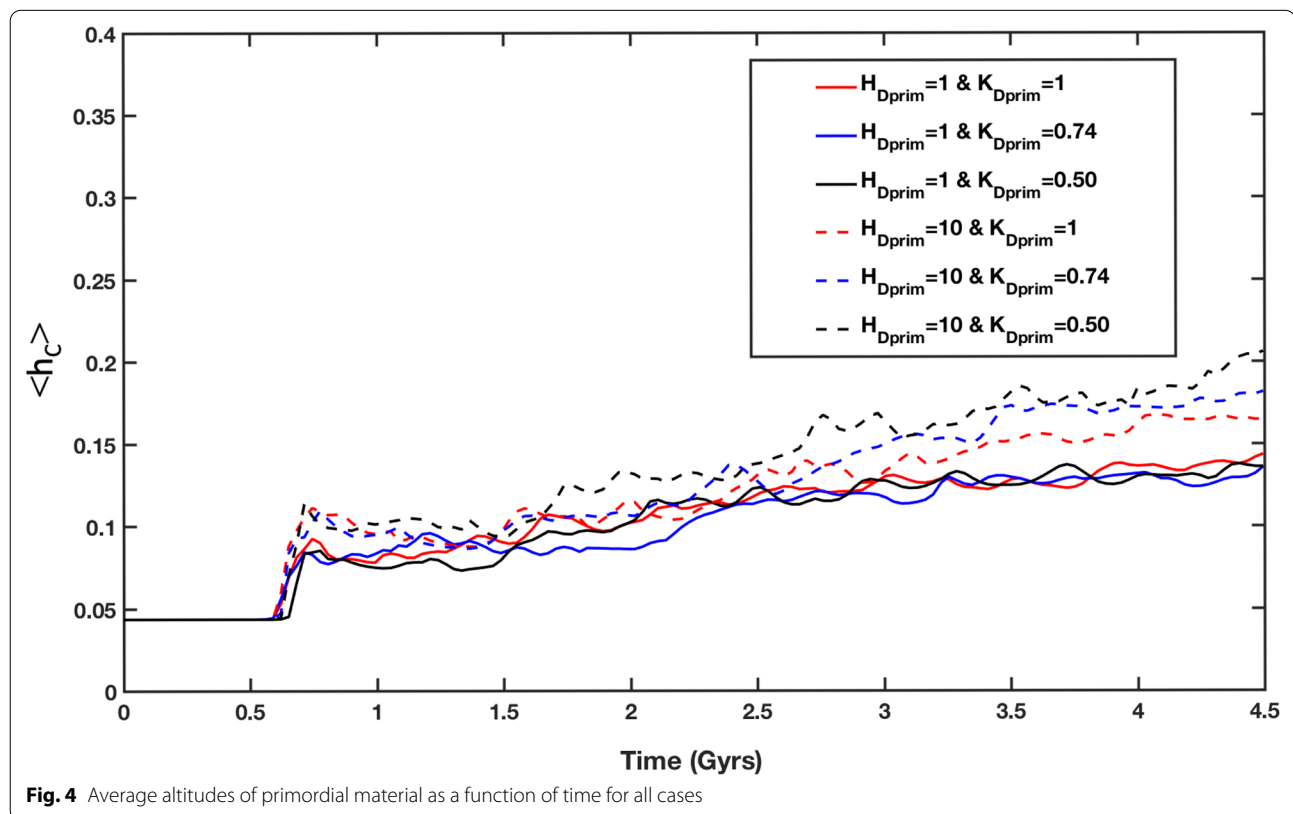
Figure 4 shows the evolution of averaged altitude of primordial material as a function of time ($\langle h_C \rangle$, refer to Eq. (6) in the Method section). The slight, regular increase in $\langle h_C \rangle$ indicates that these piles are being slowly eroded over time due to entrainment of primordial material by thermal plumes (i.e., they remain overall stable during the entire evolution, but are progressively eroded by thermal plumes that are generated at their tops). In simulations with homogeneous internal heating, the evolution of $\langle h_C \rangle$ is similar for the three values of K_{Dprim} we tested, with $\langle h_C \rangle$ increasing only slightly with time due to entrainment of primordial material by plumes. In the simulations with $H_{Dprim}=10$, $\langle h_C \rangle$ are larger and increase slightly faster with time, due to both a larger rate of entrainment by plumes and to the fact that piles get more buoyant. Furthermore, clear differences

appear depending on the thermal conductivity of primordial material with lower conductivities promoting entrainment, which leads to slightly larger values of $\langle h_C \rangle$.

Overall, our experiments indicate that reducing the thermal conductivity of piles of primordial, dense material compared to that of the surrounding mantle plays a minor role in the long-term stability of these piles. However, this influence slightly increases when the primordial materials are enriched in heat-producing elements.

Discussion

The numerical experiments performed in this study allowed a better understanding of the influence of the compositional dependence of thermal conductivity on mantle dynamics. We find that the reduction of thermal conductivity in primordial material does not strongly alter the stability and structure of these primordial reservoirs. As in previous studies (Deschamps and Tackley 2009; Li et al. 2014; McNamara and Zhong 2004), the buoyancy ratio (measuring the density contrast between primordial and ambient mantle materials) and thermal viscosity contrast remain the main controlling parameters on the long-term stability of the lower mantle reservoirs of dense primordial material, while composition-dependent thermal conductivity plays a



second-order role and does not substantially alter the pattern of mantle convection. In addition, because primordial reservoirs are hot and cover a small fraction of the CMB, and all other parameters are the same, changes in CMB heat flow are also very limited compared to the total CMB heat flow (Figs. 1c and 2c).

Although the composition-dependent thermal conductivity plays a second-order role on the long-term stability of primordial reservoirs, our study indicates some interesting side effects. As can be clearly seen from our numerical experiments, if the large primordial reservoirs are not enriched in heat-producing elements, their long-term structure and stability are not substantially altered by the composition-dependent thermal conductivity even with a reduction up to 50%. Undegassed components observed in oceanic island basalts (OIBs) are unlikely to be enriched in radiogenic elements, because they would, in the long term, produce large amounts of ^4He and result in low values of the isotopic helium ratio $^3\text{He}/^4\text{He}$ in OIB, in contradiction with observations (e.g., Hofmann 1997). By contrast, iron-rich residuals of the magma ocean crystallization from which piles of dense material may originate (e.g., Labrosse et al. 2007) may be enriched in long-lived radiogenic isotopes (Trønnes et al. 2019). Enrichment of reservoirs of primordial material in heat-producing elements may, in turn, have some influence on the long-term evolution of the Earth. Citron et al. (2020), for instance, suggests that it could influence the morphology of the primordial reservoirs, and even destabilize them. Our results further indicate that if their thermal conductivity is reduced compared to that of the ambient mantle, their morphology would be further affected, mainly resulting in a more pronounced topography. As the thermal conductivity of primordial material is reduced, heat transfer by conduction within piles is slower, while the heat influx (from the CMB) and outflux (to the regular mantle) are slightly reduced. Consequently, the secular cooling of these reservoirs slows down, and, in some cases, reservoirs may even slowly heat up. The enrichment in heat-producing elements would then enhance this heating effect, effectively cause primordial reservoirs to gain extra thermal buoyancy (compared to the ambient mantle), and therefore destabilize them gradually, as can be observed in snapshots of composition fields at the end of the simulations (Figs. 2 and 3) and from the time evolution of average altitudes of primordial material (Fig. 4). Since the chemical density contrast is large enough to overcome the thermal buoyancy by the effects mentioned above, these primordial reservoirs remain stable and persistent in mantle convection over a long period of time compared to Earth's history. However, as a result

Table 1 Root mean square (rms) of temperature differences in the bottom 200 km (ΔT_{bot}) of the models

H_{Dprim}	K_{Dprim}	$\text{rms } \Delta T_{\text{bot}} \text{ (K)}$		
		Global	Positive	Negative
1	1	507.3	526.1	485.4
1	0.74	498.7	469.0	524.9
1	0.50	491.0	485.9	491.9
10	1	600.3	673.6	530.0
10	0.74	591.2	706.4	491.7
10	0.50	623.7	742.7	517.3

of stronger thermal buoyancy caused by enrichment in heat-producing elements, they have a larger vertical extent and cover a smaller fraction of the CMB than in simulations without enrichment in heat-producing elements. To further investigate this point, we calculated the rms (root mean square) of temperature differences in the bottom 200 km (ΔT_{bot}) at 4.5 Gyrs for all the cases we run (Table 1). These calculations indicate that in cases with homogeneous internal heating, positive thermal anomalies have a smaller rms than negative thermal anomalies when K_{Dprim} is smaller than 1. By contrast, in cases with heterogeneous internal heating, we observe that, in all cases, positive thermal anomalies have a larger rms than negative thermal anomalies, indicating that reservoirs of primordial material are hotter if enriched in heat-producing elements. Interestingly this effect is slightly more pronounced as thermal conductivity of primordial material is reduced, which may be, again, related to the fact that heat transfer within the pile is slower.

While our simulations are not designed to reconstruct the mantle thermal history, they suggest that the primordial reservoirs in the lower mantle of the Earth may be cooling down more slowly than previously thought, due to slower heat diffusion within the piles. However, because it does not cause a large difference in global CMB heat flow, this effect may have a limited impact on mantle cooling. By contrast, a local minimum in heat flux within primordial reservoirs may impact core dynamics more substantially, favoring the formation of core upwellings beneath these reservoirs. Mechanical or thermal coupling between core and mantle dynamics may then further influence CMB heat flow (Yoshida and Hamano 2016; Yoshida et al. 2017).

Our results may have further implications for the evolution of seismic ultra-low velocity zones (ULVZs) observed above the CMB. If ULVZs are residues of a basal magma ocean and are enriched in heat-producing elements (Labrosse et al. 2007), their thermal

conductivity may be substantially lower than that of the ambient mantle (Hsieh et al. 2018). Although our simulations do not specifically model ULVZs and their evolution, which would require a third type of tracer for the chemical field, they suggest that these regions may have cooled down more slowly than expected, due to a large reduction in their thermal conductivity. They may still be very hot compared to the ambient mantle, and possibly partially molten. Note that, because they would be much enriched in iron, these regions may also be significantly denser LLVP and regular mantle materials. Modelling ULVZs would require a third tracer species and the prescription of additional buoyancy ratio and thermal conductivity. This should be fully investigated in future work. It should further be pointed out that because thermal conductivities of mantle minerals decrease with increasing temperature (Klemens et al. 1962), there should be positive feedback between the effects of iron enrichment and high temperature, further reducing the thermal conductivity of primordial materials. This effect is not included in our calculations. Finally, our modelled thermal conductivity profile does not consider potential iron saturation effects, where the thermal conductivity of primordial materials may saturate as the iron content is larger than a threshold value, and which has been experimentally observed in $\delta - (Al, Fe)OOH$ at the lowermost mantle pressure (Hsieh et al. 2020). A full investigation on the combined effects of temperature, pressure, and iron saturation on the thermal conductivity should, therefore, be conducted in combination with the major physical parameters controlling mantle dynamics.

Abbreviations

LLVPs: Large low velocity provinces; ULVZs: Ultra-low velocity zones; HPEs: Heat-producing elements; rms: Root mean square.

Supplementary Information

The online version contains supplementary material available at <https://doi.org/10.1186/s40623-022-01608-3>.

Additional file 1.

Acknowledgements

We are grateful to Masaki Yoshida and Bernhard Steinberger, and to the handling editor, Kiyoshi Baba, for their reviews and comments that helped to improve a first version of this manuscript. The calculations were performed on Tianhe-1(A) at National Supercomputer Center in Tianjin.

Authors' contributions

YL conceived the project; ran numerical simulations; analysed the data; and wrote the first draft. FD provided mentorship to YL and helped edit the manuscript. ZDS ran part of the simulations. PJT provided the original code StagYY. ZDS, JMG, WPH, LZ and PJT contributed to the interpretation of the results and the writing of the paper. All authors read and approved the final manuscript.

Funding

The National Natural Science Foundation of China (NSFC) Grant: 41888101 (YL and LZ.) International partnership program of Chinese Academy of Sciences Grant: 132A11KYSB20200019 (YL and LZ.) Key Research Program of the Institute of Geology and Geophysics, CAS, Grant: IGGCAS-201904 (YL.) MoST Grant: 109-2116-M-001-029 (F.D.)

Availability of data and materials

The numerical code StagYY is the property of P. J. T and ETH Zurich, and is available for collaborative studies from P. J. T. (paul.tackley@erdw.ethz.ch). Data used in this study (binary output files of StagYY) can be accessed online (<https://doi.org/10.5281/zenodo.5571607>), and the post-processing program is available upon request to the corresponding authors.

Declarations

Competing interests

The authors declare that they have no competing interests.

Author details

¹State Key Laboratory of Lithospheric Evolution, Institute of Geology and Geophysics, Institutions of Earth Science, Chinese Academy of Sciences, Beijing, China. ²Institute of Earth Sciences, Academia Sinica, Taipei, Taiwan. ³Institute of Geophysics, Department of Earth Sciences, ETH Zürich, Zürich, Switzerland.

Received: 12 January 2022 Accepted: 14 March 2022

Published: 23 March 2022

References

- Brandenburg J, Van Keken P (2007) Deep storage of oceanic crust in a vigorously convecting mantle. *J Geophys Res*. <https://doi.org/10.1029/2006JB004813>
- Christensen UR, Hofmann AW (1994) Segregation of subducted oceanic crust in the convecting mantle. *J Geophys Res* 99(B10):19867–19884. <https://doi.org/10.1029/93JB03403>
- Christensen UR, Yuen DA (1985) Layered convection induced by phase transition. *J Geophys Res* 90(B12):10291–10300. <https://doi.org/10.1029/JB090iB12p10291>
- Citron RI, Lourenço DL, Wilson AJ, Grima AG, Wipperfurth SA, Rudolph ML, Cottaar S, Montési LG (2020) Effects of heat-producing elements on the stability of deep mantle thermochemical piles. *Geochem Geophys Geosyst*. 21(4):e2019GC008895. <https://doi.org/10.1029/2019GC008895>
- Davaille A, Romanowicz B (2020) Deflating the LLVPs: bundles of mantle thermochemical plumes rather than thick stagnant “piles.” *Tectonics* 39(10):e2020TC006265. <https://doi.org/10.1029/2020TC006265>
- Davies DR, Goes S, Davies JH, Schuberth B, Bunge HP, Ritsema J (2012) Reconciling dynamic and seismic models of Earth's lower mantle: the dominant role of thermal heterogeneity. *Earth Planet Sci Lett* 353:253–269. <https://doi.org/10.1016/j.epsl.2012.08.016>
- Deschamps F, Hsieh WP (2019) Lowermost mantle thermal conductivity constrained from experimental data and tomographic models. *Geophys J Int* 219(S1):S115–S136. <https://doi.org/10.1093/gji/ggz231>
- Deschamps F, Tackley PJ (2009) Searching for models of thermo-chemical convection that explain probabilistic tomography II-Influence of physical and compositional parameters. *Phys Earth Planet Inter* 176(1–2):1–18. <https://doi.org/10.1016/j.pepi.2009.03.012>
- Deschamps F, Cobden L, Tackley PJ (2012) The primitive nature of large low shear-wave velocity provinces. *Earth Planet Sci Lett* 349:198–208. <https://doi.org/10.1016/j.epsl.2012.07.012>
- Deschamps F, Konishi K, Fuji N, Cobden L (2019) Radial thermo-chemical structure beneath Western and Northern Pacific from seismic waveform inversion. *Earth Planet Sci Lett* 520:153–163. <https://doi.org/10.1016/j.epsl.2019.05.040>
- Dziewonski AM, Lekic V, Romanowicz BA (2010) Mantle anchor structure: an argument for bottom up tectonics. *Earth Planet Sci Lett* 299(1–2):69–79. <https://doi.org/10.1016/j.epsl.2010.08.013>

- French S, Romanowicz BA (2014) Whole-mantle radially anisotropic shear velocity structure from spectral-element waveform tomography. *Geophys J Int* 199(3):1303–1327. <https://doi.org/10.1093/gji/ggu334>
- Garnero EJ, McNamara AK, Shim SH (2016) Continent-sized anomalous zones with low seismic velocity at the base of Earth's mantle. *Nat Geosci* 9(7):481–489. <https://doi.org/10.1038/ngeo2733>
- Hansen U, Yuen D, Kroening S, Larsen T (1993) Dynamical consequences of depth-dependent thermal expansivity and viscosity on mantle circulations and thermal structure. *Phys Earth Planet Inter* 77(3–4):205–223. [https://doi.org/10.1016/0031-9201\(93\)90099-U](https://doi.org/10.1016/0031-9201(93)90099-U)
- He Y, Wen L (2012) Geographic boundary of the "Pacific Anomaly" and its geometry and transitional structure in the north. *J Geophys Res.* <https://doi.org/10.1029/2012JB009436>
- Hernlund JW, Tackley PJ (2008) Modeling mantle convection in the spherical annulus. *Phys Earth Planet Inter* 171(1–4):48–54. <https://doi.org/10.1016/j.pepi.2008.07.037>
- Hofmann AW (1997) Mantle geochemistry: the message from oceanic volcanism. *Nature* 385(6613):219–229. <https://doi.org/10.1038/385219a0>
- Houser C, Masters G, Shearer P, Laske G (2008) Shear and compressional velocity models of the mantle from cluster analysis of long period waveforms. *Geophys J Int* 174:195–212. <https://doi.org/10.1111/j.1365-245X.2008.03763.x>
- Hsieh WP, Deschamps F, Okuchi T, Lin JF (2017) Reduced lattice thermal conductivity of Fe-bearing bridgmanite in Earth's deep mantle. *J Geophys Res Solid Earth* 122(7):4900–4917. <https://doi.org/10.1002/2017JB014339>
- Hsieh WP, Deschamps F, Okuchi T, Lin JF (2018) Effects of iron on the lattice thermal conductivity of Earth's deep mantle and implications for mantle dynamics. *Proc Natl Acad Sci USA* 115(16):4099–4104. <https://doi.org/10.1073/pnas.1718557115>
- Hsieh WP, Ishii T, Chao KH, Tsuchiya J, Deschamps F, Ohtani E (2020) Spin transition of iron in δ -(Al, Fe) OOH induces thermal anomalies in Earth's lower mantle. *Geophys Res Lett* 47(4):e2020GL087036. <https://doi.org/10.1029/2020GL087036>
- Ishii M, Tromp J (1999) Normal-mode and free-air gravity constraints on lateral variations in velocity and density of Earth's mantle. *Science* 285(5431):1231–1236. <https://doi.org/10.1126/science.285.5431.1231>
- Jones TD, Maguire RR, van Keken PE, Ritsema J, Koelemeijer P (2020) Subducted oceanic crust as the origin of seismically slow lower-mantle structures. *Prog Earth Planet Sci* 7:1–16. <https://doi.org/10.1186/s40645-020-00327-1>
- Kellogg LH, Hager BH, van der Hilst RD (1999) Compositional stratification in the deep mantle. *Science* 283(5409):1881–1884. <https://doi.org/10.1126/science.283.5409.1881>
- Klemens P, White G, Tainsh R (1962) Scattering of lattice waves by point defects. *Philos Mag* 7(80):1323–1335. <https://doi.org/10.1080/14786436208213166>
- Koelemeijer P, Deuss A, Ritsema J (2017) Density structure of Earth's lowermost mantle from Stoneley mode splitting observations. *Nat Commun.* <https://doi.org/10.1038/ncomms15241>
- Konishi K, Fuji N, Deschamps F (2020) Three-dimensional Elastic and Anelastic Structure of the Lowermost Mantle Beneath the Western Pacific From Finite-Frequency Tomography. *J Geophys Res Solid Earth* 125(2):e2019JB018089. <https://doi.org/10.1029/2019JB018089>
- Labrosse S, Hernlund J, Coltice N (2007) A crystallizing dense magma ocean at the base of the Earth's mantle. *Nature* 450(7171):866–869. <https://doi.org/10.1038/nature06355>
- Lau HC, Mitrovica JX, Davis JL, Tromp J, Yang HY, Al-Attar D (2017) Tidal tomography constrains Earth's deep-mantle buoyancy. *Nature* 551(7680):321–326. <https://doi.org/10.1038/nature24452>
- Lee CTA, Luffi P, Höink T, Li J, Dasgupta R, Hernlund J (2010) Upside-down differentiation and generation of a 'primordial' lower mantle. *Nature* 463(7283):930–933. <https://doi.org/10.1038/nature08824>
- Li M, McNamara AK (2018) The influence of deep mantle compositional heterogeneity on Earth's thermal evolution. *Earth Planet Sci Lett* 500:86–96. <https://doi.org/10.1016/j.epsl.2018.08.009>
- Li Y, Deschamps F, Tackley PJ (2014) The stability and structure of primordial reservoirs in the lower mantle: insights from models of thermochemical convection in three-dimensional spherical geometry. *Geophys J Int* 199(2):914–930. <https://doi.org/10.1093/gji/ggu295>
- Li Y, Deschamps F, Tackley PJ (2015) Effects of the post-perovskite phase transition properties on the stability and structure of primordial reservoirs in the lower mantle of the Earth. *Earth Planet Sci Lett* 432:1–12. <https://doi.org/10.1016/j.epsl.2015.09.040>
- Li Y, Deschamps F, Yang J, Chen L, Zhao L, Tackley PJ (2019) Effects of the compositional viscosity ratio on the long-term evolution of thermochemical reservoirs in the deep mantle. *Geophys Res Lett* 46(16):9591–9601. <https://doi.org/10.1029/2019GL083668>
- McNamara AK, Zhong S (2004) Thermochemical structures within a spherical mantle: superplumes or piles? *J Geophys Res.* <https://doi.org/10.1029/2003JB002847>
- Mosca I, Cobden L, Deuss A, Ritsema J, Trampert J (2012) Seismic and mineralogical structures of the lower mantle from probabilistic tomography. *J Geophys Res.* <https://doi.org/10.1029/2011JB008851>
- Murakami M, Hirose K, Kawamura K, Sata N, Ohishi Y (2004) Post-perovskite phase transition in MgSiO_3 . *Science* 304(5672):855–858. <https://doi.org/10.1126/science.1095932>
- Nakagawa T, Tackley PJ, Deschamps F, Connolly JA (2010) The influence of MORB and harzburgite composition on thermo-chemical mantle convection in a 3-D spherical shell with self-consistently calculated mineral physics. *Earth Planet Sci Lett* 296(3–4):403–412. <https://doi.org/10.1016/j.epsl.2010.05.026>
- Ni S, Tan E, Gurnis M, Helmberger D (2002) Sharp sides to the African superplume. *Science* 296(5574):1850–1852. <https://doi.org/10.1126/science.1070698>
- Ohta K, Yagi T, Hirose K, Ohishi Y (2017) Thermal conductivity of ferropericlase in the Earth's lower mantle. *Earth Planet Sci Lett* 465:29–37. <https://doi.org/10.1016/j.epsl.2017.02.030>
- O'Neill HSC, Palme H (2008) Collisional erosion and the non-chondritic composition of the terrestrial planets. *Philos Trans A Math Phys Eng Sci* 366(1883):4205–4238. <https://doi.org/10.1098/rsta.2008.0111>
- Ritsema J, Deuss A, Van Heijst H, Woodhouse J (2011) S40RTS: a degree-40 shear-velocity model for the mantle from new Rayleigh wave dispersion, teleseismic traveltime and normal-mode splitting function measurements. *Geophys J Int* 184(3):1223–1236. <https://doi.org/10.1111/j.1365-246X.2010.04884.x>
- Schmeling H, Marquart G, Ruedas T (2003) Pressure- and temperature-dependent thermal expansivity and the effect on mantle convection and surface observables. *Geophys J Int* 154(1):224–229. <https://doi.org/10.1046/j.1365-246X.2003.01949.x>
- Tackley PJ (1998) Three-dimensional simulations of mantle convection with a thermo-chemical basal boundary layer: D"? In: Gurnis M, Wyssession ME, Knittle E, Buffett BA (eds) *The Core-Mantle Boundary Region*. *Geodynamical Series*. Vol 28, pp 231–253. doi:<https://doi.org/10.1029/GD028p0231>
- Tackley PJ (2008) Modeling compressible mantle convection with large viscosity contrasts in a three-dimensional spherical shell using the yin-yang grid. *Phys Earth Planet Inter* 171(1–4):7–18. <https://doi.org/10.1016/j.pepi.2008.08.005>
- Tackley PJ, King SD (2003) Testing the tracer ratio method for modeling active compositional fields in mantle convection simulations. *Geochim Geophys Geosyst.* <https://doi.org/10.1029/2001GC000214>
- Tateno S, Hirose K, Sata N, Ohishi Y (2009) Determination of post-perovskite phase transition boundary up to 4400 K and implications for thermal structure in D" layer. *Earth Planet Sci Lett* 277(1–2):130–136. <https://doi.org/10.1016/j.epsl.2008.10.004>
- Tosi N, Yuen DA, Čadež O (2010) Dynamical consequences in the lower mantle with the post-perovskite phase change and strongly depth-dependent thermodynamic and transport properties. *Earth Planet Sci Lett* 298(1–2):229–243. <https://doi.org/10.1016/j.epsl.2010.08.001>
- Tosi N, Yuen DA, de Koker N, Wentzcovitch RM (2013) Mantle dynamics with pressure- and temperature-dependent thermal expansivity and conductivity. *Phys Earth Planet Inter* 217:48–58. <https://doi.org/10.1016/j.pepi.2013.02.004>
- Trampert J, Deschamps F, Resovsky J, Yuen DA (2004) Probabilistic tomography maps chemical heterogeneities throughout the lower mantle. *Science* 306(5697):853–856. <https://doi.org/10.1126/science.1101996>
- Trønnes RG, Baron MA, Eigenmann KR, Guren MG, Heyn BH, Løken A, Mohn CE (2019) Core formation, mantle differentiation and core-mantle interaction within Earth and the terrestrial planets. *Tectonophysics* 760:165–178. <https://doi.org/10.1016/j.tecto.2018.10.021>

- Wang W, Xu Y, Sun D, Ni S, Wentzcovitch R, Wu Z (2020) Velocity and density characteristics of subducted oceanic crust and the origin of lower-mantle heterogeneities. *Nat Commun* 11(1):1–8. <https://doi.org/10.1038/s41467-019-13720-2>
- Ward J, Nowacki A, Rost S (2020) Lateral velocity gradients in the African lower mantle inferred from slowness space observations of multipathing. *Geochem Geophys Geosyst* 21:e2020GC009025. <https://doi.org/10.1029/2020GC009025>
- White WM (2015) Isotopes, DUPAL, LLSVPs, and anekantavada. *Chem Geol* 419:10–28. <https://doi.org/10.1016/j.chemgeo.2015.09.026>
- Yoshida M, Hamano Y (2016) Numerical studies on the dynamics of two-layer Rayleigh-Bénard convection with an infinite Prandtl number and large viscosity contrasts. *Phys Fluids* 28:116601. <https://doi.org/10.1063/1.4966685>
- Yoshida M, Iwamori H, Hamano Y, Suetsugu D (2017) Heat transport and coupling modes in Rayleigh-Bénard convection occurring between two layers with largely different viscosities. *Phys Fluids* 29:096602. <https://doi.org/10.1063/1.4989592>
- Zhong S (2006) Constraints on thermochemical convection of the mantle from plume heat flux, plume excess temperature, and upper mantle temperature. *J Geophys Res*. <https://doi.org/10.1029/2005JB003972>

Publisher's Note

Springer Nature remains neutral with regard to jurisdictional claims in published maps and institutional affiliations.

Submit your manuscript to a SpringerOpen[®] journal and benefit from:

- Convenient online submission
- Rigorous peer review
- Open access: articles freely available online
- High visibility within the field
- Retaining the copyright to your article

Submit your next manuscript at ► [springeropen.com](https://www.springeropen.com)
